Received: 3 May 2020 | Revised: 9 September 2020 | Accepted: 12 September 2020

DOI: 10.1002/cjce.24010

THE CANADIAN JOURNAL OF CHEMICAL ENGINEERING

Canadian Society for Chemical Engineering | *For Our Future*
Société canadienne de génie chimique | *Pour notre avenir*

ARTICLE

Modelling and boundary optimal control design of hybrid column flotation

Maryam Azhin | **Khushaal Popli** | **Vinay Prasad**

Department of Chemical and Materials Engineering, University of Alberta, Edmonton, Alberta, Canada

Correspondence
Vinay Prasad, Department of Chemical and Materials Engineering, University of Alberta, 12th Floor, Donadeo Innovation Centre for Engineering (ICE), 9211-116 Street, Edmonton, AB T6G 1H9, Canada.
Email: vprasad@ualberta.ca

Funding information
Jaffer Professorship in Process Systems and Control Engineering; Natural Sciences and Engineering Research Council of Canada, Grant/Award Number: RGPIN-2019-04600

Abstract

A three-phase continuous hybrid flotation column that seeks to obtain the benefits of both mechanical cells and flotation columns is modelled as the interconnection of a CSTR representing the well-mixed zone and two plug-flow reactors (PFR) representing pulp and froth zones. The plant model accounts for the micro-scale processes such as bubble-particle collision and attachment and the appearance and breakage of bubbles. This complex distributed parameter system (DPS) is described by sets of nonlinear coupled conservation counter-current hyperbolic partial differential equations (PDEs) and one set of ordinary differential equations (ODEs). The dynamic conservation law-based model for the continuous hybrid flotation column including well-stirred, pulp (bubbly), and froth zones, is utilized in an optimal model-based controller design. This linear quadratic regulator (LQR)-based controller accounts for optimality, stability, and performance. The controller design utilizes a linear model obtained by linearization at operating steady states of interest. A full-state optimal feedback control law is designed and controller performance has been demonstrated through a numerical simulation of physically meaningful and relevant plant operating conditions. The LQR-based optimal controller outperforms proportional-integral (PI)-based control by more than an order of magnitude in terms of a return to steady state after a perturbation in the initial condition.

KEYWORDS

boundary control, distributed-lumped parameter system, hyperbolic PDEs, LQ control

1 | INTRODUCTION

Column flotation is an efficient separation process to separate valuable mineral(s) from ore(s) based on the differences in minerals' hydrophobicity. Modern flotation columns were developed in Canada in the early 1960s,[1] and since their commercial application in the 1980s,[2] they have been used in a broad range of applications in the mineral processing industry, including for metallic and non-metallic ores, as well as in wastewater treatment processes. Technological advantages of this separation technique over conventional mechanical flotation cells include simplicity of construction, low energy consumption, and higher recovery and product grade.[3] In general, minerals, water, and air are fed in the lower part of the column. Subsequently, the transport of the material and minerals is affected by the hydrodynamics of the inflow and outflow streams and includes the transport of hydrophobic particles attached to the bubbles (which propagate in an attached form from the pulp to the froth zone) along with up-flow and down-flow of the liquid (in its free form). Note that the net downward flow of

liquid represents the so-called bias of the flotation column. Column flotation is a complex distributed parameter system (DPS) that involves three phases of solid particles, gas or air bubbles, and liquid flows (up-flow and down-flow).

The main operational objective of column flotation is to maximize the grade and/or recovery of valuable mineral(s) while keeping the other variable above a threshold value, and the main objective of column flotation control is to maintain its required operational level in the presence of disturbances. However, large variations in the feed concentrations and several other hydrodynamical disturbances reduce the grade and recovery of column operation. Therefore, control strategies and system analyses applied to column flotation typically target down-flow, froth depth, grade, recovery, and gas hold up by manipulating variables such as the flow of feed, air, and wash-water, as well as reagent addition.[4-6] Currently, a common control approach in flotation plants is the knowledge-based (eg, fuzzy logic or supervisory) control realization, despite the fact that the computational cost of rule-based control for such a complex system is high.[7] Model-based control design has the potential to provide improved performance while ensuring stability of the hydrodynamic system. Due to the presence of a large number of variables and subprocesses, the modelling of the flotation process is complex.[8] Although setting clear boundaries is often not possible, models of the flotation process can be classified as fundamental (based on first principles models, eg, probabilistic, kinetic, and population-balance), empirical (statistical models derived from experimental data) and hybrid (based on both experimental data and first principles models). First principles models employ the conservation of mass and the mechanisms related to bubble-bubble and bubble-particle interactions occurring in the mechanical flotation cells. In contrast, empirical modelling is realized by adjusting the parameters in a regression relationship to provide the best fit to the existing data, with considerable flexibility in choosing the functional form of the regression relationship. Hybrid models are determined with a mix of empirical and fundamental relationships.[9]

Although several models have been proposed for mechanical froth flotation cells,[10–12] there are only a few dynamic models proposed for the column flotation process in the literature that can be used for model-based controller design applications. These models try to connect the hydrodynamic process conditions (interfacial area of bubbles, bubble size distribution, and particle size distribution) to mineral recovery and provide an improvement to the theoretical understanding of column flotation.[13–18] Some of these models can be classified as micro-scale models,[19,20] implying that they were developed to estimate design parameters for a column flotation system, such as particle velocity[21] and gas dispersion,[22,23] and not for use in process control.

Initial modelling efforts for column flotation include the work of Sastry and Lofftus[15] and Cruz,[14] who proposed a population balance-based model for the flotation column process. This model was based on the microscopic and macroscopic description of pulp and froth zones in which bubble coalescence and loading have been considered and a distribution of bubble sizes, particle sizes, and particle types were also used. Non-constant attachment and detachment rates in Cruz,[14] were defined by the probability of attachment and detachment of particles from the bubbles. The column was modelled based on a vertical combination of a perfectly mixed aeration zone, an ideal CSTRs-in-series lower collection zone, a single perfectly mixed feed zone, an ideal CSTRs-in-series upper collection zone, the interface, and three plug flow volumes including stabilized froth, wash water, and draining froth. This dynamic simulator of the column flotation system did not have the ability to handle pulp level variations or to account for pressure effects in the gas phase. On the other hand, the model proposed by Bouchard et al[24] is based on macroscopic descriptions of pulp and froth phases, material balance, and a first-order kinetic assumption for attachment/detachment. This model uses a CSTRs-in-series approach with the ability to handle pulp level variations and account for pressure effects in the gas phase. In addition, a mean bubble diameter in every simulation cell is used and the physical mechanisms of collision, attachment, and detachment have not been considered separately in determining the attachment and detachment rate constants. In Yahui et al,[25] a hyperbolic transport-reaction system based on the model published by Sastry and Lofftus[15] is considered, which accounts only for froth and collection zones. Along similar lines, other works have considered conservative hyperbolic PDEs in a physically meaningful laboratory setting.[26,27]

Flotation is generally effective over a size range of approximately 15-150 μm of mineral particles.[28] Mechanical flotation cells provide enhanced particle-bubble collision through agitation, while flotation columns have a large quiescent zone that enables fractionation. In this regard, in order to expand the range of particle separation, and to combine the advantages of both types of flotation approaches, our group has constructed and is testing a novel hybrid flotation column. In addition to enhanced bubble-particle collision, the use of an impeller in the well-mixed section also results in the production of smaller bubbles, which is favourable for the attachment of fine particles, while the quiescent area of the column is favourable for the separation of coarser minerals. In this work, we present a model to be used in the development

of a controller for this hybrid flotation column. Note that the term hybrid in this work implies that a CSTR is added to the flotation column. The three-phase dynamic model for the hybrid column accounts for the coupling of a nonlinear hetero-directional system of hyperbolic PDEs-ODE in which the upward and downward liquid flows represent flows of free particles. The gas flow represents the flow of attached hydrophobic particles to the bubbles. The model accounts for three regions: well-mixed (CSTR), pulp (collection), and froth (cleaning), as well as micro-scale processes taking place in the column, such as bubble-particle collisions and attachments and the hydrodynamic forces in the liquid.

As mentioned earlier, fundamental model-based control design can provide improved performance while guaranteeing stability. In particular, an optimal control approach such as one based on linear quadratic regulator (LQR) design, can provide (nominal) exponential stabilization for the system over a wide range of operating conditions, which is not necessarily possible with empirical models and/or proportional-integral-derivative (PID) control. While model predictive control (MPC) would be the preferred approach for real-time optimal control, it should be pointed out that this is a nonlinear infinite-dimensional system that presents significant computational challenges for the implementation of MPC. This motivates the choice of an LQR-based optimal controller, the implementation of which will provide insights for the future design of a model predictive controller.

The hybrid flotation column is an example of a transport-reaction system and typically, in-domain actuation, is applied for the purpose of controlling such systems (eg, heating the fixed bed reactor through the jacket along the column). Developing controller design for such models representing these systems is challenging and has received some attention in the literature.[29] However, in most transport-reaction systems (including column flotation), control actuation is applied at the boundaries of the system, which increases the complexity of the design further. The mathematical difficulty of solving boundary control problems is associated with dealing with the point actuation (at the boundary); to solve the control problem for these systems, we have transferred the actuation to in-domain actuation.[30] However, there is limited published research in the area of optimal control for this type of system. Moghadam et al[30] considered the optimal control of coupled ordinary differential equations (ODEs) and hyperbolic partial differential equations (PDEs) with uni-directional transport in a two-phase contactor with a constant transport velocity.

The novelty of this contribution, besides the derivation of a dynamic fundamental model for a hybrid column flotation process that accounts for bubble-particle bubble-bubble interactions, is in extending the framework of an optimal control formulation for PDEs from the literature.[31-36] Specifically, the model for the novel hybrid column flotation system represents a three-phase hetero-directional transport system where the velocity matrix in the transport operator is spatially and temporally varying along the column height (see Figure 1), and the optimal control formulation is developed by extending the framework of Moghadam et al.[30]

We provide a systematic general procedure for the design of a full state optimal controller regarding the coupling of nonlinear hetero-directional system of hyperbolic PDE-ODE. We consider a boundary coupled hetero-directional nonlinear hyperbolic PDE-ODE system that allows the inclusion of various transport interactions, systematic dynamical analysis of the linearized model, and design of optimal feedback operators for the coupled PDE-ODE system by solving Riccati matrix operator equations. Accordingly, optimal control gains of the ODE subsystem given by a finite dimensional model and infinite dimensional hetero-directional hyperbolic PDEs are coupled and solved simultaneously. In this sense, one can explore optimality of the state evolution and control effort evolution that is compartmentalized in different sections of the column system. In addition, we provide a comparison with non-model based (PI) controllers, and we point out advantages of the proposed design. Also, the

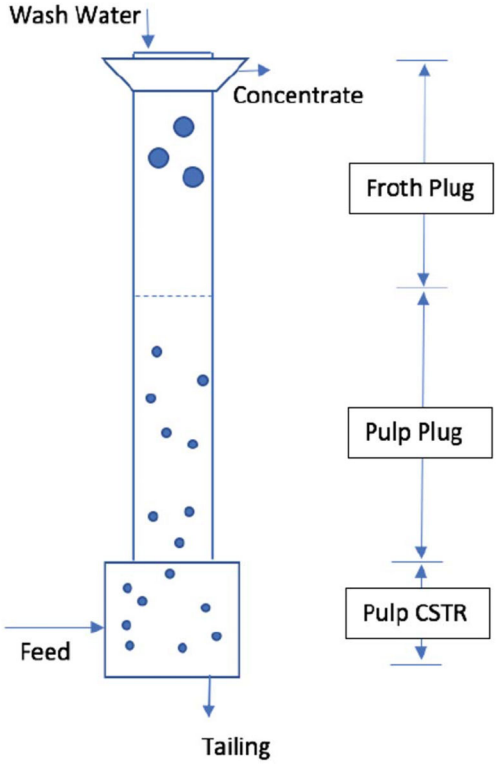

FIGURE 1 Schematic of the hybrid flotation column

grade and recovery are directly related to the states of the model at the top of the column and the LQR controller design aims at stabilizing a constant reference state, which achieves regulation of desired grade or recovery.

Thus, the major contribution of this work is the investigation of the control of a novel hybrid column flotation process and the development of an optimal controller for a boundary coupled hetero-directional nonlinear hyperbolic PDE-ODE system.

This paper is structured as follows: in section 1, the column flotation process is described and, in section 2, is modelled as a system of nonlinear coupled PDE-ODEs, and a linearized state-space description for the system is obtained. Section 3 addresses state feedback regulator design. The profile of the linearized system is illustrated and parameters for regulators are designed and calculated in detail in section 4, and the simulation results are shown to demonstrate the controller performance. Finally, section 5 provides conclusions from the study.

2 | MODEL DEVELOPMENT FOR HYBRID COLUMN FLOTATION

2.1 | Hybrid column

A common column flotation apparatus consists of two zones: the pulp (collection) and the froth (cleaning) zones. The hybrid column we consider is unique since an impeller has been added to the column flotation geometry (see Figure 1). Assuming perfect mixing, the compartment with the agitation is considered as a continuous stirred tank reactor (CSTR). On the other hand, the collection zone (pulp) and the bubbly zone (froth) in the column section are considered as two plug flow reactors (PFRs) in series, in which we assume perfect radial mixing and no axial mixing (along the direction of the flow). In this modelling framework, the effect of axial dispersion is neglected in comparison to the flow of the fluid. A seminal paper by Sastry and Lofftus[15] in 1988 revealed that for estimating the degree of dispersion in flotation columns, the Peclet number for plug flow conditions can be considered to be infinite.

The dynamic mathematical model has been developed considering bubble-particle attachment and detachment, as well as gas and liquid transport phenomena. The process can be considered as a counter-current flow system. The air injected by a sparger at the bottom of the column forms bubbles that rise up through the column length. Slurry that contains the particles of the ore is introduced in the agitated section. After collision and contact between the bubbles and minerals, hydrophobic minerals attach to the bubbles and form bubble-particle aggregates. The valuable minerals (ie, hydrophobic particles) are transported to the top of the column by the bubbles and finally overflow from top of the column as the product (concentrate). The purpose of the wash water above the overflow level is to wash down entrained (hydrophilic) particles back to the froth zone.[37,38] Therefore, the interaction between rising bubbles, entrained particles, and down-flow slurry leads to mass transfer of the particles between the water and air phases as well as between the upward and downward water flows. The mass transfer processes of attachment and detachment of particles to and from the bubbles are treated as kinetic processes or reactions.

2.2 | Modelling

We present a three-phase fundamental dynamic model based on physical principles for a hybrid flotation column operated as a continuous process (ie, with continuous inflow and outflow) that includes a well-mixed section. The model extends the modelling contributions in the literature.[14,24,26,39] The novelty of this contribution is that it has been tailored for a hybrid flotation column, accounts for a CSTR added to the column geometry, includes transport-reaction conservation laws, and accounts for macro- and micro-scale processes, including bubble-particle interactions and mass transfer between up-flow and down-flow. As illustrated in Figure 2, this process is modelled as an interconnection of three different subsystems, including a CSTR, which represents a well-mixed zone, and two plug flow transport reactors, representing pulp and froth zones. In addition, the model is augmented by considering the microscale processes taking place in the column, such as bubble-particle collisions and attachment, as well as hydrodynamic forces. In particular, the modelling accounts for the three phases: solid particles, gas (air bubbles), and liquid in the froth zone. The three flows in the system are the gas upward flow, liquid up-flow, and liquid down-flow. A solid particle can be found in any of the eight compartments (I, II, III, III', IV, V, V′, VI), based on its state (eg, attached to the bubbles (gas phase) as X_2 in the CSTR, X_5 in the pulp, and X_8 in the froth zone). A solid particle can be free (not attached) in the downward liquid flow as X_3 in the pulp or as X_6 in the froth or as X_1 in the CSTR, or as X_4 or X_7 in liquid phase up-flow, in the pulp or froth zones, respectively.

In addition, a mass balance-based nonlinear model representing the reaction term in the transport-reaction system is defined for valuable particles (hydrophobic) for each compartment. Although the model formulation is provided in detail, experimental validation of the model

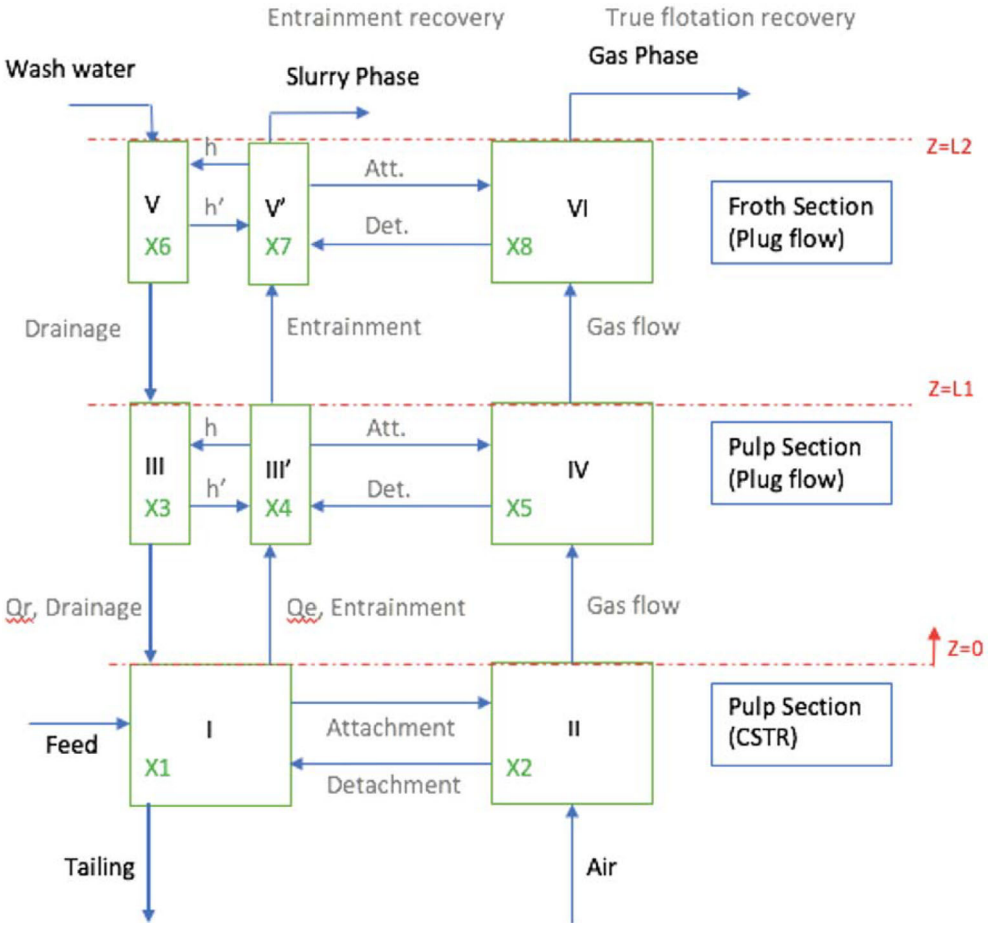

FIGURE 2 Schematic of a three-phase column flotation system considering the transport of hydrophobic particles

is being realized and will be addressed in subsequent reports. The assumption of regulated and constant pulp/froth interface position (ie, level) is applied. As reported in previous studies,[2] the most important factors in level regulation are the feed and tailing flow rates, which are kept constant in our framework. The resulting model equations, a system of nonlinear hyperbolic PDEs and ODEs have been solved using Euler integration backward in space and forward in time such that the numerical stability of the simulation is preserved.

2.2.1 | A three-phase model for hydrophobic particles in the CSTR

The state variables for the CSTR model are concentration of valuable minerals attached to the bubbles, $X_2(t)$, and free in the liquid phase, $X_1(t)$. A mass balance over the CSTR control volume, a lumped parameter system (LPS), provides the following:

$$\frac{dX_1}{dt} = -\frac{(Q_t + Q_{ep})X_1}{V_c(1-\varepsilon_c)} - K_{ac}X_1 + K_{dc}X_2 + \frac{Q_f X_{1,0}}{V_c(1-\varepsilon_c)} \quad (1)$$

$$\frac{dX_2}{dt} = -\frac{Q_a X_2}{V_c \varepsilon_c} + K_{ac}X_1 - K_{dc}X_2 \quad (2)$$

where $X_{1,0}$ denotes the input (concentration of free particles) into the CSTR, and the balance of the flow rates provides the following relationship for the stationary operating processes: $Q_f + Q_r = Q_t + Q_e$ (see Nomenclature list).

2.2.2 | Hydrophobic particles model in the pulp zone

The state variables for the pulp or collection zone are the concentrations of the valuable mineral attached to the bubbles, $X_5(z, t)$, free in the up-flow, $X_4(z, t)$, and free in the down-flow, $X_3(z, t)$. Transport hyperbolic PDEs are used to describe the evolution of transport in both directions. The transport of attached and free valuable materials in the air and up-flow streams is linked to the states of the CSTR by the boundary conditions:

$$\frac{\partial X_3}{\partial t} = \frac{Q_{rp}}{A_c \alpha_p (1-\varepsilon_p)} \frac{\partial X_3}{\partial z} - K_{ap3} X_3 + kK_{dp} X_5 + h(X_4 - X_3) \quad (3)$$

$$B.C.\ at\ z = L_1 \qquad X_3(L_1, t) = X_6(L_1, t) \quad (4)$$

where $X_3(z, t)$ is the state that represents particles transported downwards and is defined on the height range of $[0, L_1]$. Therefore, the concentration of the attached and free valuable materials transported upwards are as follows:

$$\frac{\partial X_4}{\partial t} = -\frac{Q_{ep}}{A_c (1-\alpha_p)(1-\varepsilon_p)} \frac{\partial X_4}{\partial z} - K_{ap4} X_4 + (1-k) K_{dp} X_5 - h'(X_4 - X_3) \quad (5)$$

$$\frac{\partial X_5}{\partial t} = -\frac{Q_a}{A_c \varepsilon_p} \frac{\partial X_5}{\partial z} + K_{ap3} X_3 + K_{ap4} X_4 - K_{dp} X_5 \quad (6)$$

with the associated boundary conditions that are linked to the states of the CSTR:

$$B.C.\ at\ z = 0 \qquad X_4(0, t) = X_1(t) \quad (7)$$

$$B.C.\ at\ z = 0 \qquad X_5(0, t) = X_2(t) \quad (8)$$

The states $X_4(z, t)$ and $X_5(z, t)$ are also defined on $[0, L_1]$. At this point, there is a coupling of the CSTR dynamics to the underlying transport PDE through the boundary conditions, so that the dynamics of the CSTR concentration drive the boundary states evolution for the transport of the upward ($X_4(z, t)$ and $X_5(z, t)$) and downward ($X_3(z, t)$) particles, driven by the state $X_6(z, t)$ from the froth zone.

2.2.3 | Hydrophobic particles model in the froth and interface zones

The state variables for the froth zone are concentration of the valuable mineral attached to the bubbles ($X_8(z, t)$), free valuable minerals in the up-flow ($X_7(z, t)$), and free valuable minerals in the down-flow ($X_6(z, t)$) with associated boundary conditions:

$$\frac{\partial X_6}{\partial t} = \frac{(Q_{rf} + Q_w)}{A_c \alpha_f (1-\varepsilon_f)} \frac{\partial X_6}{\partial z} - K_{af6} X_6 + k_2 K_{df} X_8 + h_f (X_7 - X_6) \quad (9)$$

$$B.C.\ at\ z = L_2 \qquad X_6(L_2, t) = \eta(t) \quad (10)$$

where the conditions at the top of the column are associated with the wash water input $\eta(t)$. The upward transport includes free and attached particles, which is coupled to the pulp zone by boundary conditions and is given as follows:

$$\frac{\partial X_7}{\partial t} = -\frac{Q_{ef}}{A_c (1-\alpha_f)(1-\varepsilon_f)} \frac{\partial X_7}{\partial z} - K_{af7} X_7 + (1-k_2) K_{df} X_8 - h'_f (X_7 - X_6) \quad (11)$$

$$\frac{\partial X_8}{\partial t} = -\frac{Q_a}{A \varepsilon_f} \frac{\partial X_8}{\partial z} + K_{af6} X_6 + K_{af7} X_7 - K_{df} X_8 \quad (12)$$

$$B.C.\ at\ z = L_1;\ X_7(L_1, t) = X_4(L_1, t) \quad (13)$$

$$B.C.\ at\ z = L_1;\ X_8(L_1, t) = X_5(L_1, t) \quad (14)$$

2.2.4 | Gas-holdup model for froth and pulp zones

In this section, we describe gas fraction models in the pulp and froth zones, in which gas holdup variations propagate both temporally and spatially along the column height. The model accounts for the bubble coalescence and breakage of three bubble size classes in the pulp and three bubble size classes in the froth:

$$\frac{\partial \varepsilon_{p,n}(z,t)}{\partial t} = -v_{\varepsilon,n,p} \frac{\partial \varepsilon_{p,n}(z,t)}{\partial z} - \mathcal{D}_{p,n}(z,t) + \mathcal{A}_{p,n}(z,t); \quad (15)$$

$$\frac{\partial \varepsilon_{f,n}(z,t)}{\partial t} = -v_{\varepsilon,n,f} \frac{\partial \varepsilon_{f,n}(z,t)}{\partial z} - \mathcal{D}_{f,n}(z,t) + \mathcal{A}_{f,n}(z,t) \quad (16)$$

$$\varepsilon_{p,n}(0,t) = \varepsilon_{c,n}(t), \quad \varepsilon_p(z,t) = \sum_{n=1}^{3} \varepsilon_{p,n}(z,t) \quad (17)$$

$$\varepsilon_{f,n}(L_1,t) = \varepsilon_{p,n}(L_1,t), \quad \varepsilon_f(z,t) = \sum_{n=1}^{3} \varepsilon_{f,n}(z,t) \quad (18)$$

The total gas hold-up is a summation of the gas hold-ups of the three bubbles size classes. In the present work, based on the approaches taken in the works of Sastry,[39,40] and extended by Cruz,[14] the total increase/decrease in the volume fraction of bubbles is defined in terms of the total rise, $\mathcal{A}_{p,n}(z,t)$, and the total decline, $\mathcal{D}_{p,n}(z,t)$, which are measures of how many interactions result in coalescence in each bubble size class n that could be applied to the entire column:

$$\mathcal{A}_{i,n}=0.5\sum_{j}^{Nl}\Psi_{i,n-j,j}\frac{\varepsilon_{n-j}\varepsilon_j}{\sum_{l}^{Nl}\frac{\varepsilon_l Db_{n-j}^3 Db_j^3}{Db_n^3 Db_l^3}},\ j<n \tag{19}$$

$$\mathcal{D}_{i,n}=\sum_{j}^{Nl}\Psi_{i,n,j}\frac{\varepsilon_n\varepsilon_j}{\sum_{l}^{Nl}\varepsilon_l\frac{Db_j^3}{Db_l^3}} \tag{20}$$

Nl is the total number of discrete size classes in the distribution, $l\neq 0$. The collision success factor, Ψ, is an experimentally defined parameter that is a function of the sizes of the colliding bubbles[14]:

$$\Psi_{i,n,j}=\xi_{i,n,j}\left(Db_n+Db_j\right)^{-2} \tag{21}$$

In the system of Equations (1)-(3), (5), (6), (9), (11), and (12), the grade and recovery of the froth overflow (the concentrate or product flow) is controlled by three inputs: the slurry composition at the top of the column, $U_1=\eta$, which is linked to the wash water flow rate; the feed composition, $U_2=X_{1,0}$; and the air flow rate, $U_3=Q_a$, which will be considered in the full state feedback control design. It is assumed that feed composition is manipulated by dilution of the inlet slurry. In general, density is often changed by adjusting the water added in the grinding and flotation circuit. The grade entering the flotation circuit is occasionally changed by changing the blend of the feed upstream, and also manipulating the recycle stream in the flotation circuit.

The state space model of the CSTR can be written in a matrix format as follows:

$$\frac{\partial}{\partial t}\begin{bmatrix}X_1\\X_2\end{bmatrix}=\begin{bmatrix}\frac{-\left(Q_t+Q_{ep}\right)}{V_c(1-\varepsilon_c)}-K_{ac} & K_{dc}\\ K_{ac} & -K_{dc}-\frac{Q_a}{\varepsilon_c V_c}\end{bmatrix}\begin{bmatrix}X_1\\X_2\end{bmatrix}+\begin{bmatrix}\frac{Q_f X_{1,0}}{V_c(1-\varepsilon_c)}\\0\end{bmatrix} \tag{22}$$

It is assumed that $K_{ac}=GU_3^m$ where $m=0.45$ and $G=8.08$, and $U_2=X_{1,0}$. Therefore, Equation (22) can be rewritten as follows:

$$\frac{\partial X_1}{\partial t}=\left(\frac{-\left(Q_t+Q_{ep}\right)}{V_c(1-\varepsilon_c)}-GU_3^m\right)X_1+K_{dc}X_2+\frac{Q_f U_2}{V_c(1-\varepsilon_c)} \tag{23}$$

$$\frac{\partial X_2}{\partial t}=GU_3^m X_1-\left(K_{dc}+\frac{U_3}{V_c\varepsilon_c}\right)X_2 \tag{24}$$

The compact model of the transport PDE-ODE interconnection given in the state space format for the froth zone is given below:

$$\frac{\partial}{\partial t}\begin{bmatrix}X_6\\X_7\\X_8\end{bmatrix}+\Lambda_1\frac{\partial}{\partial z}\begin{bmatrix}X_6\\X_7\\X_8\end{bmatrix}=\Gamma_1\begin{bmatrix}X_6\\X_7\\X_8\end{bmatrix} \tag{25}$$

while equations for the collection zone or pulp zone can be written in the state space format as follows:

$$\frac{\partial}{\partial t}\begin{bmatrix}X_3\\X_4\\X_5\end{bmatrix}+\Lambda_2\frac{\partial}{\partial z}\begin{bmatrix}X_3\\X_4\\X_5\end{bmatrix}=\Gamma_2\begin{bmatrix}X_3\\X_4\\X_5\end{bmatrix} \tag{26}$$

The transport and reaction matrices for Equations (25) and (26) are defined as follows:

$$\Lambda_1=\begin{bmatrix}\frac{-(Q_r+Q_w)}{A_c\alpha_f(1-\varepsilon_f)} & 0 & 0\\ 0 & \frac{Q_e}{A_c(1-\alpha_f)(1-\varepsilon_f)} & 0\\ 0 & 0 & \frac{Q_a}{A_c\varepsilon_f}\end{bmatrix} \tag{27}$$

$$\Gamma_1=\begin{bmatrix}-K_{af6}-h_f & h_f & k_2K_{df}\\ h_f' & -K_{af7}-h_f' & (1-k_2)K_{df}\\ K_{af6} & K_{af7} & -K_{df}\end{bmatrix} \tag{28}$$

$$\Lambda_2=\begin{bmatrix}\frac{-Q_r}{A_c\alpha_p(1-\varepsilon_p)} & 0 & 0\\ 0 & \frac{Q_e}{A_c(1-\alpha_p)(1-\varepsilon_p)} & 0\\ 0 & 0 & \frac{Q_a}{A_c\varepsilon_p}\end{bmatrix} \tag{29}$$

$$\Gamma_2=\begin{bmatrix}-K_{ap3}-h & h & kK_{dp}\\ h' & -K_{ap4}-h' & (1-k)K_{dp}\\ K_{ap3} & K_{ap4} & -K_{dp}\end{bmatrix} \tag{30}$$

$$\frac{\partial}{\partial t}\begin{bmatrix}\varepsilon_{p,n}\\\varepsilon_{f,n}\end{bmatrix}=\begin{bmatrix}V_{\varepsilon,n,p}\frac{\partial}{\partial z} & 0\\ 0 & V_{\varepsilon,n,f}\frac{\partial}{\partial z}\end{bmatrix}\begin{bmatrix}\varepsilon_{p,n}\\\varepsilon_{f,n}\end{bmatrix}+\begin{bmatrix}\mathcal{A}_{p,n}-\mathcal{D}_{p,n}\\ \mathcal{A}_{f,n}-\mathcal{D}_{f,n}\end{bmatrix} \tag{31}$$

Finally, the boundary and initial conditions for the PDEs and ODEs are given by the following:

$$X_4(0,t) = X_1(t);\ X_5(0,t) = X_2(t) \tag{32}$$

$$X_3(L_1,t) = X_6(L_1,t);\ X_7(L_1,t) = X_4(L_1,t) \tag{33}$$

$$X_8(L_1,t) = X_5(L_1,t);\ X_6(L_2,t) = \eta(t) \tag{34}$$

$$X_1(0) = X_{1,0};\ X_2(0) = 0;\ X_3(z,0) = X_{3,0}(z) \tag{35}$$

$$;X_4(z,0) = X_{4,0}(z);\ X_5(z,0) = X_{5,0}(z) \tag{36}$$

$$\varepsilon_{p,n}(0,t) = \varepsilon_{c,n}(t); \varepsilon_{f,n}(L_1,t) = \varepsilon_{p,n}(L_1,t) \tag{37}$$

$$\varepsilon_{p,n}(z,0) = \varepsilon_{p,n,0}(z); \varepsilon_{f,n}(z,0) = \varepsilon_{f,n,0}(z); \varepsilon_{c,n}(0) = \varepsilon_{c,n,0} \tag{38}$$

The coupling of the PDE-ODE system is provided through the boundaries between the CSTR and the pulp (linking the ODE system and the transport hyperbolic PDE) and through the boundary between the pulp and froth zones. For simplicity, we do not consider dropback of particles from the column to the CSTR, but there is no conceptual issue in including this phenomenon if required.

2.3 | Linearized Model

The system of model equations developed above is nonlinear, and it is linearized around the steady state of interest to facilitate dynamic analysis and controller design. Note that the controller developed based on this linearized model is implemented on the nonlinear process. The equilibrium condition for the system is obtained by solving the set of nonlinear PDEs and ODEs for the plant model at steady state. With the given steady state inputs, the steady state spatial profiles of the gas hold up and concentration of particles in three forms, as attached, free upward, and free downward are illustrated in Figures 3 and 4. Hence, the linear system is obtained by defining the standard perturbation of the states around the steady state:

$$x_k(t) = X_k(t) - X_{kss};\quad k = 1\ \ to\ \ 2 \tag{39}$$

$$x_j(z,t) = X_j(z,t) - X_{jss}(z);\quad j = 3\ \ to\ \ 8 \tag{40}$$

$$\tilde{u}_\nu(t) = U_\nu(t) - U_{\nu,ss};\quad \nu = 1\ \ to\ \ 3 \tag{41}$$

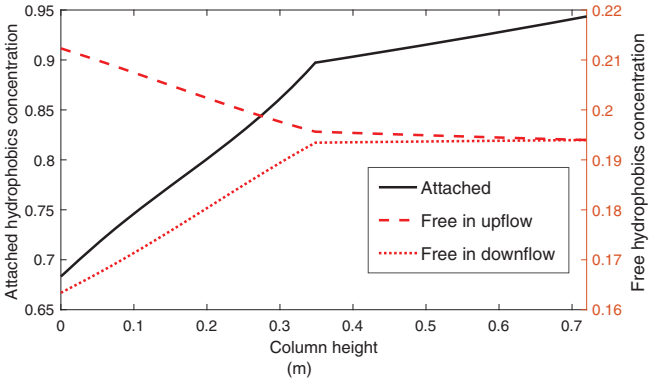

FIGURE 3 The steady state concentration profiles through the column obtained by the simulation of the full nonlinear model: $X_{5ss}([0, L_1])$-$X_{8ss}([L_1, L_2])$, solid line: $X_{4ss}([0, L_1])$-$X_{7ss}([L_1, L_2])$, dashed line; and $X_{3ss}([0, L_1])$-$X_{6ss}([L_1, L_2])$, dotted line

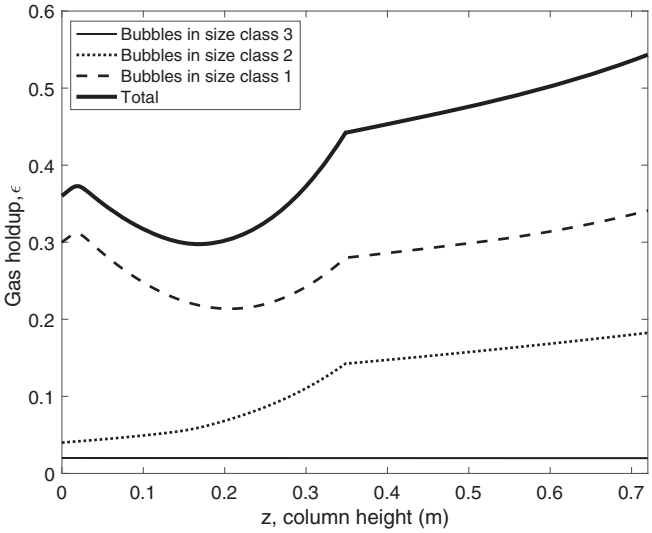

FIGURE 4 Schematic of the steady state gas hold up profiles through the column

which provides the following linearized system of equations:

$$\frac{\partial}{\partial t}\begin{bmatrix} x_1 \\ x_2 \end{bmatrix} = \begin{bmatrix} A_{111ss} & A_{112ss} \\ A_{121ss} & A_{122ss} \end{bmatrix}\begin{bmatrix} x_1 \\ x_2 \end{bmatrix} + + \begin{bmatrix} \dfrac{Q_f \tilde{u}_2}{V_c(1-\varepsilon_c)} - GmU_{3ss}^{m-1} X_{1ss} \tilde{u}_3 \\ \left(GmU_{3ss}^{m-1} X_{1ss} - \dfrac{X_{2ss}}{\varepsilon_c V_c}\right)\tilde{u}_3 \end{bmatrix} \tag{42}$$

$$\frac{\partial x_3(z,t)}{\partial t} = V_3 \frac{\partial x_3(z,t)}{\partial z} + A_{211} x_3(z,t) + A_{212} x_4(z,t) + + A_{213} x_5(z,t) \tag{43}$$

$$\frac{\partial x_4(z,t)}{\partial t} = -V_4\frac{\partial x_4(z,t)}{\partial z} + A_{221}x_3(z,t) + \\ + A_{222}x_4(z,t) + A_{223}x_5(z,t) \tag{44}$$

$$\frac{\partial x_5(z,t)}{\partial t} = \frac{-U_{3ss}}{\varepsilon_p A_c}\frac{\partial x_5(z,t)}{\partial z} + A_{231}x_3(z,t) + \\ + A_{232}x_4(z,t) + A_{233}x_5(z,t) - \frac{1}{\varepsilon_p A_c}\frac{\partial X_{5ss}(z)}{\partial z}\tilde{u}_3 \tag{45}$$

$$\frac{\partial x_6(z,t)}{\partial t} = V_6\frac{\partial x_6(z,t)}{\partial z} + A_{311}x_6(z,t) + A_{312}x_7(z,t) + \\ + A_{313}x_8(z,t) \tag{46}$$

$$\frac{\partial x_7(z,t)}{\partial t} = -V_7\frac{\partial x_7(z,t)}{\partial z} + A_{321}x_6(z,t) + \\ + A_{322}x_7(z,t) + A_{323}x_8(z,t) \tag{47}$$

$$\frac{\partial x_8(z,t)}{\partial t} = \frac{-U_{3ss}}{\varepsilon_f Ac}\frac{\partial x_8(z,t)}{\partial z} + A_{331}x_6(z,t) + \\ + A_{332}x_7(z,t) + A_{333}x_8(z,t) - \frac{1}{\varepsilon_f Ac}\frac{\partial X_{8ss}(z)}{\partial z}\tilde{u}_3 \tag{48}$$

During linearization of the model given by Equations (1)-(12), it is considered that $V_5 = \frac{U_3}{\varepsilon_p A_c}$ and $V_8 = \frac{U_3}{\varepsilon_f A_c}$ are the functions of the third input to the system ($Q_a = U_3$):

$$V_3 = \frac{Q_r}{A_c\alpha_p(1-\varepsilon_p)};\ V_4 = \frac{Q_e}{A_c(1-\alpha_p)(1-\varepsilon_p)} \tag{49}$$

$$V_5 = \frac{Q_a}{A_c\varepsilon_p};\ V_6 = \frac{(Q_r+Q_w)}{A_c\alpha_f(1-\varepsilon_f)} \tag{50}$$

$$V_7 = \frac{Q_e}{A_c(1-\alpha_f)(1-\varepsilon_f)};\ V_8 = \frac{Q_a}{A_c\varepsilon_f} \tag{51}$$

$$A_{111ss} = \frac{-1^*(Q_t+Q_e)}{V_c(1-\varepsilon_c)} - GU_{3ss}^m \tag{52}$$

$$A_{112ss} = K_{dc};\ A_{121ss} = GU_{3ss}^m \tag{53}$$

$$A_{122ss} = -K_{dc} - \frac{U_{3ss}}{\varepsilon_c V_c} \tag{54}$$

$$A_{211} = -K_{ap3} - h;\ A_{212} = h;\ A_{213} = kK_{dp} \tag{55}$$

$$A_{221} = h';\ A_{222} = -K_{ap4} - h';\ A_{223} = (1-k)K_{dp} \tag{56}$$

$$A_{231} = K_{ap3};\ A_{232} = K_{ap4};\ A_{233} = -K_{dp} \tag{57}$$

$$A_{311} = -K_{af6} - h_f;\ A_{312} = h_f;\ A_{313} = k_2K_{df} \tag{58}$$

$$A_{321} = h_{f'};\ A_{322} = -K_{af7} - h_{f'} \tag{59}$$

$$A_{323} = (1-k_2)K_{df};\ A_{331} = K_{af6} \tag{60}$$

$$A_{332} = K_{af7};\ A_{333} = -K_{df} \tag{61}$$

with the boundary conditions $x_3(L_1, t) = x_6(L_1, t)$; $x_4(0, t) = x_1(t)$; $x_5(0, t) = x_2(t)$; $x_6(L_2, t) = \eta(t)$; $x_7(L_1, t) = x_4(L_1, t)$, and $x_8(L_1, t) = x_5(L_1, t)$.

Here, the domain of the states $x_3(z, t)$, $x_4(z, t)$, and $x_5(z, t)$ is given on $z \in (0, L_1)$, while $(x_6(z, t), x_7(z, t), x_8(z, t))$ belong to $z \in (L_1, L_2)$; hence, the challenge is to represent the entire linear state space in a compact and unified setting. Hence, the extended state $x \in L_2(0, L_1) \oplus L_2(L_1, L_2) \oplus \mathbb{R}^n$ has been considered, where X are real Hilbert spaces $L_2(0, L_1) \oplus L_2(L_1, L_2)$ with a defined inner product $\langle \cdot, \cdot \rangle$ and $\mathbb{R}^n$ is a real space. The input $u(t) \in U$, the output $y(t) \in Y$, and U and Y are real Hilbert spaces. Equations (42)-(49) can be expressed in equivalent state space format as

$$\frac{\partial x_d}{\partial t}(z,t) = V(z)\frac{\partial x_d}{\partial z}(z,t) + M(z)x_d(z,t) + \\ + B_d(z)u(t) \tag{62}$$

$$\frac{\partial x_l}{\partial t}(t) = Ax_l(t) + Bu(t) \tag{63}$$

$$y(t) = C(\cdot)[x_d(\cdot,t), x_l(t)]^T \tag{64}$$

augmented with the boundary conditions and initial conditions:

$$x_d = [x_d^{\mathcal{F}}; x_d^{\mathcal{P}}] \tag{65}$$

$$x_d^{\mathcal{F}}(L_1,t) = x_d^{\mathcal{P}}(L_1,t);\ x_d^{\mathcal{P}}(0,t) = x_l(t) \tag{66}$$

$$x_d(z,0) = x_{d,0}(z);\ x_l(0) = x_{l,0} \tag{67}$$

$C(\cdot) = diag(C_d(\cdot), C_l)$, $x_d(\cdot, t) = [x_6, x_7, x_8, x_3, x_4, x_5]^T$, and $x_l(t) = [x_1\ x_2]$. The input array $u = [\eta, \tilde{u}_2, \tilde{u}_3]$ will be considered in the full state feedback control design.

2.4 | Boundary to in-domain input transformation

The interconnection of the system of hyperbolic PDEs and ODEs is considered as a boundary-controlled

hyperbolic PDE system. In particular, the inputs are applied to the ODE system and by the boundary interconnection propagate to the pulp and the froth zones; however, one input is applied in the counter-current direction at the top of the column (eg, η). The manipulated inputs are wash water, air flow rate, and feed concentration, and the controlled variables are the spatial profiles of the minerals. In order to change the inhomogeneous boundary condition for the PDE system to the new system with a homogeneous boundary condition, one can apply a state transformation by considering $\omega^{\mathcal{P}}(z,t)=x_d^{\mathcal{P}}(z,t)-\mathfrak{B}^{\mathcal{P}}x_l(t)$ and $\omega^{\mathcal{F}}(z,t)=x_d^{\mathcal{F}}(z,t)-\mathfrak{B}^{\mathcal{F}}x_d^{\mathcal{P}}(L_1,t)$ (we drop z-dependence in $\omega^{\mathcal{F}}(z,\ t)\ =\ \omega^{\mathcal{F}}(t)$ and $\omega^{\mathcal{P}}(z,t)=\omega^{\mathcal{P}}(t)$ in subsequent sections). In this way, the state of the CSTR given by the ODEs is linked to the spatial state of the pulp section by the $\mathfrak{B}$ operator, and from the interface of the pulp-froth section to the froth section. In other words, the spatial functions $\mathfrak{B}^{\mathcal{F}}$ and $\mathfrak{B}^{\mathcal{P}}$ represent two actuator distribution functions which link the finite dimensional CSTR state, $x_l(t)$, to $\omega^{\mathcal{P}}(z,t)$ and $x_d^{\mathcal{P}}(L_1,t)$ to $\omega^{\mathcal{F}}(z,\ t)$, respectively. Using this transformation, the control variable $U(t)$ can affect the PDEs throughout the entire column domain:

$$\dot{\omega}^{\mathcal{F}}(t)=\dot{x}_d^{\mathcal{F}}(t)-\mathfrak{B}^{\mathcal{F}}\dot{x}_d^{\mathcal{P}}(L_1,t) \tag{68}$$

$$\dot{\omega}^{\mathcal{P}}(t)=\dot{x}_d^{\mathcal{P}}(t)-\mathfrak{B}^{\mathcal{P}}\dot{x}_l(t) \tag{69}$$

$$\omega(0)=\omega_0;\ \ \omega_0=\left[\omega_0^{\mathcal{F}};\ \ \omega_0^{\mathcal{P}}\right];\ \ x_d=\left[x_d^{\mathcal{F}};x_d^{\mathcal{P}}\right] \tag{70}$$

where $\omega_0^{\mathcal{P}}=x_{d,0}^{\mathcal{P}}-\mathfrak{B}^{\mathcal{P}}x_{l,0}$ and $\omega_0^{\mathcal{F}}=x_{d,0}^{\mathcal{F}}-\mathfrak{B}^{\mathcal{F}}x_{d,0}^{\mathcal{P}}(L_1)$. Hence, $\dot{\omega}^{\mathcal{F}}(t)=\dot{x}_d^{\mathcal{F}}(t)-\mathfrak{B}^{\mathcal{F}}\left(\omega^{\mathcal{P}}(L_1,t)+\mathfrak{B}^{\mathcal{P}}\dot{x}_l\right)$, so that the ODE dynamics couple to the froth and pulp zones in the column. Therefore, the result of this state transformation is a newly obtained infinite-dimensional state-space system of coupled DPS and LPS:

$$\dot{x}(t)=\mathcal{A}x(t)+\mathcal{B}u(t) \tag{71}$$

$$y(t)=\mathfrak{C}x(t) \tag{72}$$

The system operator $\mathcal{A}$ contains the linear operator $\mathcal{F}$ which is defined as $\mathcal{F}h(z)=V(z)\frac{dh(z)}{dz}+M(z)h(z)$ on its domain, which is defined as $D(\mathcal{F})$ as follows:

$$\left\{\begin{array}{c}\left[x_6,x_7,x_8,x_3,x_4,x_5\right]^T\in X: x\ is\ abs.\ cont.\\ \frac{dx_j}{dz}\in X, j=3,4,5,6,7,8\\ x_6(L_2,t)=\eta, x_7(L_1,t)=x_4(L_1,t),\\ x_8(L_1,t)=x_5(L_1,t), x_3(L_1,t)=x_6(L_1,t),\\ x_4(0)=x_1, x_5(0)=x_2\end{array}\right\} \tag{73}$$

where $X=\mathscr{L}_2(L_1,L_2)\times\mathscr{L}_2(0,L_1)$, and the operator of the coupled system takes the following form:

$$\mathcal{A}=\begin{bmatrix}\mathcal{F} & \mathfrak{A}\\ 0 & A\end{bmatrix} \tag{74}$$

on the extended infinite and finite dimensional space $X\times R^2$:

$$\begin{bmatrix}\dot{\omega}(t)\\ \dot{x}_l(t)\end{bmatrix}=\begin{bmatrix}\mathcal{F} & \mathfrak{A}\\ 0 & A\end{bmatrix}\begin{bmatrix}\omega(t)\\ x_l(t)\end{bmatrix}+\begin{bmatrix}\bar{\mathcal{B}}_d\\ B\end{bmatrix}u(t) \tag{75}$$

$$y(t)=\mathfrak{C}\left[\omega(t)\ \ x_l(t)\right]^T \tag{76}$$

The state transformations that transfer the boundary to in-domain actuations are achieved by considering the following:

$$x_3(z,t)=x_3^n(z,t)+B_3(z)x_6(L_1,t) \tag{77}$$

$$x_4(z,t)=x_4^n(z,t)+B_4(z)x_1(t) \tag{78}$$

$$x_5(z,t)=x_5^n(z,t)+B_5(z)x_2(t) \tag{79}$$

$$x_6(z,t)=x_6^n(z,t)+B_6(z)\eta \tag{80}$$

$$x_7(z,t)=x_7^n(z,t)+B_7(z)x_4(L_1,t) \tag{81}$$

$$x_8(z,t)=x_8^n(z,t)+B_8(z)x_5(L_1,t) \tag{82}$$

which provides a condition to calculate the boundary values of B_3, B_4, B_5, B_6, B_7, and B_8.

$$x_3(L_1,t)=x_3^n(L_1,t)+B_3(L_1)x_6(L_1,t) \tag{83}$$

$$x_3(L_1,0)=x_{3,0}^n+B_3(z)x_6(L_1,0);\ x_3^n(L_1,t)=0; \tag{84}$$

$$\begin{array}{c}B_3(L_1)=1\\ x_4(0,t)=x_4^n(0,t)+B_4(0)x_1(t)\end{array} \tag{85}$$

$$x_4(z,0)=x_{4,0}^n+B_4(z)x_1(t);\ x_4^n(0,t)=0; \tag{86}$$

$$\begin{array}{c}B_4(0)=1\\ x_5(0,t)=x_5^n(0,t)+B_5(0)x_2(t)\end{array} \tag{87}$$

$$x_5(z,0)=x_{5,0}^n+B_5(z)x_2(t);\ x_5^n(0,t)=0; \tag{88}$$

$$\begin{array}{c}B_5(0)=1\\ x_6(L_2,t)=x_6^n(L2,t)+B_6(L_2)\eta(t)\end{array} \tag{89}$$

$$x_6(L_2,0) = x_{6,0}^n + B_6(z)\eta(0);\ x_6^n(L_2,t) = 0; \tag{90}$$

$$\begin{aligned} B_6(L_2) &= 1 \\ x_7(L_1,t) &= x_7^n(L_1,t) + B_7(L_1)x_4(L_1,t) \end{aligned} \tag{91}$$

$$x_7(z,0) = x_{7,0}^n + B_7(z)x_4(L_1,0);\ x_7^n(L_1,t) = 0; \tag{92}$$

$$\begin{aligned} B_7(L_1) &= 1 \\ x_8(L_1,t) &= x_8^n(L_1,t) + B_8(L_1)x_5(L_1,t) \end{aligned} \tag{93}$$

$$\begin{aligned} &x_8(z,0) = x_{8,0}^n + B_8(z)x_5(L_1,0);\ x_8^n(0,t) = 0; \\ &B_8(0) = 1 \end{aligned} \tag{94}$$

By introducing x_3, x_4, x_5, x_6, x_7, and x_8 with the above new state representations, one obtains the operators of the linear state space model. Assuming that $\mathfrak{B}$ exists, one can define a system that has a homogenous boundary condition and distributed actuation through the domain. Therefore, by taking $B_3(L_1) = 1$, $B_4(0) = 1$, $B_5(0) = 1$, $B_6(L_2) = 1$, $B_7(L_1) = 1$, and $B_8(0) = 1$, and with the assumption of $\mathfrak{B}(z) = 1$, the state space representation can be simplified as follows:

$$\mathcal{F} = \begin{bmatrix} F_{11} & F_{12} & F_{13} & 0 & F_{15} & F_{16} \\ F_{21} & F_{22} & F_{23} & F_{24} & F_{25} & F_{26} \\ F_{31} & F_{32} & F_{33} & F_{34} & F_{35} & F_{36} \\ F_{41} & F_{42} & F_{43} & F_{44} & F_{45} & F_{46} \\ F_{51} & 0 & 0 & F_{54} & F_{55} & F_{56} \\ F_{61} & 0 & 0 & F_{64} & F_{65} & F_{66} \end{bmatrix} \tag{95}$$

$$\mathfrak{A} = \begin{bmatrix} A_{311} & 0 & 0 \\ A_{321} & A_{111ss} - A_{222} & A_{112ss} - A_{223} \\ A_{331} & A_{121ss} - A_{232} & A_{122ss} - A_{233} \\ -A_{311} & A_{212} & A_{213} \\ 0 & A_{222} - A_{111ss} & A_{223} - A_{112ss} \\ 0 & A_{232} - A_{121ss} & A_{233} - A_{122ss} \end{bmatrix} \tag{96}$$

$$A = \begin{bmatrix} 0 & 0 & 0 \\ 0 & A_{111ss} & A_{112ss} \\ 0 & A_{121ss} & A_{122ss} \end{bmatrix} \tag{97}$$

$$B = \begin{bmatrix} 1 & 0 & 0 \\ 0 & \dfrac{Q_f}{V_c(1-\varepsilon_c)} & -GmU_{3ss}^{m-1}X_{1ss} \\ 0 & 0 & GmU_{3ss}^{m-1}X_{1ss} - \dfrac{X_{2ss}}{\varepsilon_c V_c} \end{bmatrix} \tag{98}$$

$$\bar{\mathcal{B}}_d = \begin{bmatrix} -1 & 0 & 0 \\ 0 & \dfrac{Q_f}{V_c(1-\varepsilon_c)} & GmU_{3ss}^{m-1}X_{1ss} \\ 0 & 0 & \mathcal{B}_{f1} \\ 1 & 0 & 0 \\ 0 & \dfrac{Q_f}{V_c(1-\varepsilon_c)} & GmU_{3ss}^{m-1}X_{1ss} \\ 0 & 0 & \mathcal{B}_{f2} \end{bmatrix} \tag{99}$$

where $\mathcal{B}_{f1} = GmU_{3ss}^{m-1}X_{1ss} - \frac{X_{2ss}}{V_c\varepsilon_c} + \frac{\partial X_{5ss}(L_1)}{\varepsilon_p A_c \partial z_p} - \frac{\partial X_{8ss}}{\varepsilon_f A_c \partial z_f}$, $\mathcal{B}_{f2} = -GmU_{3ss}^{m-1}X_{1ss} + \frac{X_{2ss}}{V_c\varepsilon_c} - \frac{1}{\varepsilon_p A_c}\frac{\partial X_{5ss}(z)}{\partial z_p}$, and $\delta(L_1 - z)$ denotes a Dirac function which takes the value of the state at the point L_1 within the domain $[0, l]$ ($l = L_1 + L_2$ being the total length of the column). It is assumed that the process is operated at a constant volume, which implies that a level controller is implemented. This state space representation accounts for infinite and finite dimensional systems. The operator $\mathcal{A}$ in Equation (71) generates an exponentially stable semigroup $T_{\mathcal{A}}(t)$ on $X \times R^2$, which means that the initial value problem for Equation (71) is well-posed and has a unique solution. Detailed expressions for the elements of $\mathcal{F}$ are provided in Appendix A.

3 | BOUNDARY OPTIMAL (LQ) REGULATOR DESIGN OF A HYBRID SYSTEM OF COUPLED HYPERBOLIC PDES AND ODES

We used the proposed optimal control law to regulate the concentration of minerals in the CSTR, and their profiles in the pulp and the froth zones:

$$\begin{bmatrix} \dot{\omega}(t) \\ \dot{x}_l(t) \end{bmatrix} = \begin{bmatrix} \mathcal{F} & \mathfrak{A} \\ 0 & A \end{bmatrix} \begin{bmatrix} \omega(t) \\ x_l(t) \end{bmatrix} + \begin{bmatrix} \bar{\mathcal{B}}_d \\ B \end{bmatrix} u(t) \tag{100}$$

$$y(t) = \mathfrak{C}[\omega(t)\ \ x_l(t)]^T \tag{101}$$

with the following boundary and initial conditions:

$$\omega(0,t) = 0;\ \ x_l(0) = x_{l,0} \tag{102}$$

where the new infinite-dimensional state-space system has a spatial state of $\omega(\cdot, t)$ and a finite dimensional of $x_l(t)$ defined as follows:

$$\omega(t) = [x_6^n\ \ x_7^n\ \ x_8^n\ \ x_3^n\ \ x_4^n\ \ x_5^n]^T \tag{103}$$

$$x_l(t) = [x_1 \;\; x_2]^T; \quad u(t) = [\eta \;\; \tilde{u}_2 \;\; \tilde{u}_3]^T \tag{104}$$

so that the combined state is a column vector, $x(t) = [\omega(t) \;\; x_l(t)]^T$. Considering the following infinite-time horizon quadratic objective function:

$$J(x_0,u) = \int_0^\infty (<\mathfrak{C}x(t), \mathcal{P}\mathfrak{C}x(t)> + <u(t), \mathcal{R}u(t)>)dt \tag{105}$$

and the positive semidefinite operator $\mathcal{P}$:

$$\mathcal{P} = PI; \quad P = \begin{bmatrix} P_{11} & P_{12} \\ P_{21} & P_{22} \end{bmatrix} \tag{106}$$

and the positive definite matrix R, one can consider the solution of the infinite horizon optimal control problem by solving the following:

$$\min_{u(t)} J = \int_0^\infty (<\mathfrak{C}x(t), \mathcal{P}\mathfrak{C}x(t)> + <u(t), \mathcal{R}u(t)>)dt \tag{107}$$

$$s.t. \dot{x}(t) = \mathcal{A}x(t) + \mathcal{B}u(t) \tag{108}$$

The minimization of the objective function results in solving the following operator Riccati equation (ORE):

$$(\mathcal{A}^*\mathcal{Q} + \mathcal{Q}\mathcal{A} + \mathfrak{C}^*\mathcal{P}\mathfrak{C} - \mathcal{Q}\mathcal{B}R^{-1}\mathcal{B}^*\mathcal{Q})x = 0 \tag{109}$$

$$u_{opt}(t) = \mathcal{K}x(t) \tag{110}$$

$$\mathcal{K} = -R^{-1}\mathcal{B}^*\mathcal{Q} \tag{111}$$

where the operator $\mathcal{A} + \mathcal{B}\mathcal{K}$ generates an exponentially stable C_0–semigroup, or, in other words, the closed-loop feedback structure through the gain $\mathcal{K}$ achieves exponential stabilization of the system. Moreover, to solve the ORE, it is assumed that the solution is in the following form:

$$\mathcal{Q} = \begin{bmatrix} \phi_0 I & 0 \\ 0 & \psi_0 I \end{bmatrix} \tag{112}$$

where ϕ_0 and ψ_0 are non-negative diagonal and non-negative symmetric matrices containing spatial functions $\phi_0(z)$ and values ψ_0, respectively. By substituting for operators $\mathcal{A}$, $\mathcal{B}$, $\mathfrak{C}$, and $\mathcal{Q}$ in Equation (109), one obtains the following:

$$\begin{bmatrix} \mathcal{F}^* & 0 \\ \mathfrak{A}^T & A^T \end{bmatrix}\begin{bmatrix} \phi_0 & 0 \\ 0 & \psi_0 \end{bmatrix} + \begin{bmatrix} \phi_0 & 0 \\ 0 & \psi_0 \end{bmatrix}\begin{bmatrix} \mathcal{F} & \mathfrak{A} \\ 0 & A \end{bmatrix} + \\ + \begin{bmatrix} \mathcal{C}_d^* & 0 \\ \bar{\mathcal{B}}_d^*\mathcal{C}_d^* & \mathcal{C}_l^* \end{bmatrix}\begin{bmatrix} P_{11} & P_{12} \\ P_{21} & P_{22} \end{bmatrix}\begin{bmatrix} \mathcal{C}_d & \mathcal{C}_d\bar{\mathcal{B}}_d \\ 0 & \mathcal{C}_l \end{bmatrix} + \tag{113}$$

$$-\begin{bmatrix} \phi_0 & 0 \\ 0 & \psi_0 \end{bmatrix}\begin{bmatrix} \bar{\mathcal{B}}_d \\ B \end{bmatrix}R^{-1}\begin{bmatrix} \bar{\mathcal{B}}_d^* & B^* \end{bmatrix}\begin{bmatrix} \phi_0 & 0 \\ 0 & \psi_0 \end{bmatrix} = 0 \tag{114}$$

Thus, matrix multiplication yields the following system of four equations:

$$\mathcal{F}^*\phi_0 + \phi_0\mathcal{F} + \mathcal{C}_d^*P_{11}\mathcal{C}_d - \phi_0\bar{\mathcal{B}}_dR^{-1}\bar{\mathcal{B}}_d^*\phi_0 = 0 \tag{115}$$

$$\phi_0\mathfrak{A} + \mathcal{C}_d^*P_{11}\mathcal{C}_d\bar{\mathcal{B}}_d + \mathcal{C}_d^*P_{12}\mathcal{C}_l + \\ -\phi_0\bar{\mathcal{B}}_dR^{-1}B^*\psi_0 = 0 \tag{116}$$

$$\mathfrak{A}^T\phi_0 + \bar{\mathcal{B}}_d^*\mathcal{C}_d^*P_{11}\mathcal{C}_d + \mathcal{C}_l^*P_{21}\mathcal{C}_d + \\ -\psi_0BR^{-1}\bar{\mathcal{B}}_d^*\phi_0 = 0 \tag{117}$$

$$A^T\psi_0 + \psi_0A + \mathfrak{B}^*\mathcal{C}_d^*P_{11}\mathcal{C}_d\mathfrak{B} + \mathcal{C}_d^*P_{21}\mathcal{C}_d\mathfrak{B} + \\ + \mathfrak{B}^*\mathcal{C}_d^*P_{12}\mathcal{C}_l + \mathcal{C}_l^*P_{22}\mathcal{C}_l - \psi_0BR^{-1}B^*\psi_0 = 0 \tag{118}$$

Since Equation (117) can be transformed to Equation (118) by taking the transpose and vice versa, these two equations are not independent. Equation (115) can be converted to the following differential equation:

$$V\frac{d\phi_0}{dz} = M^*\phi_0 + \phi_0M + \mathcal{C}_d^*P_{11}C_d + \\ -\phi_0\bar{\mathcal{B}}_dR^{-1}\bar{\mathcal{B}}_d^*\phi_0 \tag{119}$$

Therefore, the following set of equations needs to be solved to find ϕ_0:

$$V_6\frac{\partial\phi_{01}}{\partial z} = 2A_{311}\phi_{01} + P_{111} - \frac{\phi_{01}^2}{R_1} \tag{120}$$

$$-V_7\frac{\partial\phi_{02}}{\partial z} = 2A_{322}\phi_{02} + P_{112} + \\ -\phi_{02}^2\left(\left(\frac{Qf}{V_c(1-\varepsilon_c)}\right)^2\frac{1}{R_2} + \Gamma_1^2\frac{1}{R_3}\right) \tag{121}$$

$$-V_8\frac{\partial\phi_{03}}{\partial z}=2A_{333}\phi_{03}+P_{113}-\frac{\phi_{03}^2\Gamma_2^2}{R_3} \tag{122}$$

$$V_3\frac{\partial\phi_{04}}{\partial z}=2A_{211}\phi_{04}+P_{114}-\frac{\phi_{04}^2}{R_1} \tag{123}$$

$$-V_4\frac{\partial\phi_{05}}{\partial z}=2A_{222}\phi_{05}+P_{115}+ -\phi_{05}^2\left(\left(\frac{Qf}{V_c(1-\varepsilon_c)}\right)^2\frac{1}{R_2}+\Gamma_1^2\frac{1}{R_3}\right) \tag{124}$$

$$-V_5\frac{\partial\phi_{06}}{\partial z}=2A_{233}\phi_{06}+P_{116}-\frac{\phi_{06}^2}{R_3}\Gamma_3^2 \tag{125}$$

with boundary conditions:

$$\phi_{01}(L_1)=0,\ \phi_{02}(L_2)=0,\ \phi_{03}(L_2)=0,\ \phi_{04}(0)=0 \\ \phi_{05}(L_1)=0,\ \phi_{06}(L_1)=0 \tag{126}$$

where $\Gamma_1=GmU_{3ss}^{m-1}X_{1ss}$, $\Gamma_2=GmU_{3ss}^{m-1}X_{1ss}-\frac{X_{2ss}}{V_p\varepsilon_c}+\frac{1}{\varepsilon_pA_c}\frac{\partial X_{5ss}(L1)}{\partial z_p}-\frac{1}{\varepsilon_fA_c}\frac{\partial X_{8ss}}{\partial z_f}$, and $\Gamma_3=-GmU_{3ss}^{m-1}X_{1ss}+\frac{X_{2ss}}{V_c\varepsilon_c}-\frac{1}{\varepsilon_pAc}\frac{\partial X_{5ss}(L1)}{\partial z_p}$. The spatial characteristics of the gain, in the procedure of designing the LQ control law, is given in Figure 5. It should be noted that ϕ_1, ϕ_2, ϕ_3, ϕ_4, ϕ_5, and ϕ_6 are positive gains related to the states x_6, x_7, x_8, x_3, x_4, and x_5, respectively. It can be seen that the gains, Φ_{01} and Φ_{04}, associated with the states in the down-flow, x_3 and x_6, are higher than the gains associated with the states in the up-flows (entrainment and attached to the bubbles). In other words, from a practical point of view, it is more difficult to control the down-flow than the up-flows in the column flotation process. This is natural because the natural flow is the upward transport by the bubbles as the carrier and the down-flow is effected only by a small flow of the wash water. Moreover, the actuation in the pulp zone (see Figure 5) requires stronger gain than in the froth zone, Φ_{01} and Φ_{04}. Φ_{03} and Φ_{06} are the spatial gains related to the attached states in the froth and pulp, x_8 and x_5, respectively. Φ_{02} and Φ_{05} are the spatial gains related to the free entrained states, x_7 and x_4. By comparing these gains, it is clear that the control of attached particles is more difficult than the control of free entrained particles. Therefore, x_8 and x_5 require higher gains. We follow the algorithm proposed in Moghadam et al[30] to solve differential algebraic DAE Equations (119)-(125) in a systematic manner:

- First, positive symmetric matrices P_{11} and R are chosen in order to find the unique and non-negative solution of ϕ_0. Therefore, the matrix Riccati differential Equation (115) has been solved using the Euler integration method in space by solving a boundary value problem.
- After calculating ϕ_0, and choosing a guess for P_{12}, P_{22} is substituted by $P_{12}^*P_{11}^{-1}P_{12}+\varepsilon I$, $\varepsilon>0$ in Equation (119) to calculate ψ_0 and P_{12}. (Moghadam et al[30] prove that

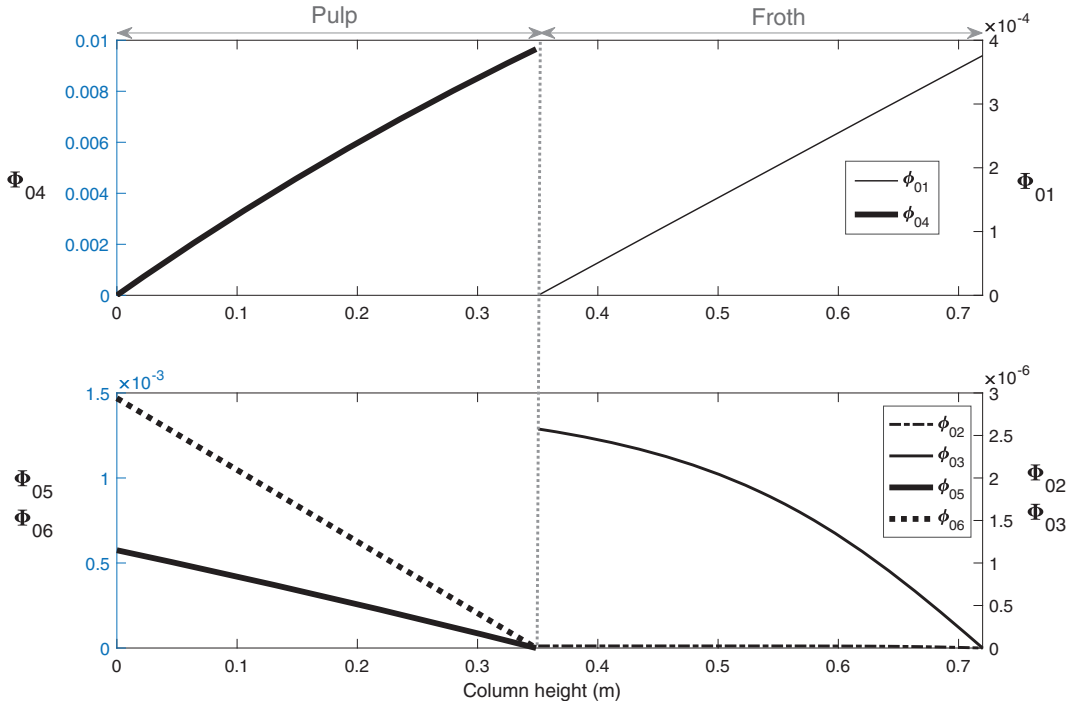

FIGURE 5 Spatial characteristics of the gain

there exists a positive symmetric P_{22} such that algebraic Equations (118) and (119) simultaneously yield solutions P_{12} and ψ_0). Note that since Equations (117) and (118) are the adjoint of each other and $P_{12} = P_{21}^*$, only one of these equations needs to be solved.

- Given P_{12}, a new $P_{22} > P_{12}^* P_{11}^{-1} P_{12} + \varepsilon I$ is chosen and Equations (118) and (119) are solved to find a new Ψ_0. The calculated P_{12} is such that the matrix P is positive and $Q = diag(\Phi_0, \Psi_0)$ (see Figure 5) is a non-negative solution of ORE.
- Finally, the state feedback operator can be calculated from the following:

$$K = -R^{-1}\left[\bar{\mathcal{B}}_d^* \phi \quad B^* \psi\right] \tag{127}$$

Note that this solution exists if the finite-dimensional part is exponentially stabilizable and exponentially detectable.

- The LQR input can be calculated using the following:

$$u_{opt} = Kx(t) \tag{128}$$

Remark. In this design, it is assumed that all states in the flotation column are measured; thus, $C_d(z)$ is equal to $diag(1,1,1,1,1,1)$ and C_l is equal to $diag(1,1,1)$. However, one can apply spatial measurements and this will only change the evaluation of the above expressions and not the design procedure. Also, the development of an observer or an estimator can provide dynamic estimates of all the states; however, given that this is a nonlinear system, it should be noted that a separation principle cannot be applied for the designs of the controller and the observer. We do not explore estimation in this work.

4 | RESULTS AND DISCUSSION

To evaluate the performance of the control strategy, the designed feed-back controller has been applied to the original nonlinear system in closed loop. The nonlinear PDE-ODE system has been integrated numerically with the Euler method, backward in space and forward in time. We present representative simulations in this section, but have tested the controller for a variety of initial conditions. Details of the parameters used in the simulations are provided in Appendix B. In the simulation study, the following values were used as one representation of the initial conditions: $x_1(0) = 0.2\ kg/m^3$, $x_2(0) = 0$, $x_3(z, 0) = 0.1066\ kg/m^3$, $x_4(z, 0) = 0.18\ kg/m^3$, $x_5(z, 0) = 0.3\ kg/m^3$, $x_6(z, 0) = 0.08\ kg/m^3$, $x_7(z, 0) = 0.18\ kg/m^3$, and $x_8(z, 0) = 0.2\ kg/m^3$. Note that the obtained steady state profiles are provided in Figures 3 and 4.

Finally, in order to account for the presence of noise, which is associated with the real plant condition, we tested the controller performance when random noise was added to the states and parameters (ie, K_{ac}) of the plant model. For the design of the optimal controller, we chose positive definite

$$P_{11} = diag(0.05, 0.0004, 0.0005, 0.0005, 0.000\,003, 0.000\,001) \tag{129}$$

and $R = diag(1,1,1)$, and

$$P_{12} = \begin{bmatrix} 0.05 & 0 & 0 \\ 0 & 0.025 & 0 \\ 0 & 0 & 0.14 \\ 0.0001 & 0 & 0 \\ 0 & 0.1 & 0 \\ 0 & 0 & 0.001 \end{bmatrix} \tag{130}$$

and calculated the positive definite matrix $P_{22} = diag(1.1,3335.9,41.2)$. Moreover, the solution to Equation (127) is the feedback controller gain.

Finally, in order to analyze the performance of the designed optimal controller, the rate of convergence of the system states after perturbation has been compared among these three cases: open-loop, controlled with model-based controller (LQR), and controlled with non-model-based (PI) controller.

Figure 6 (top) illustrates the spatial-temporal propagation of the free hydrophobic particles in the up-flow (entrainment) through the column. Figure 6 (bottom) demonstrates the spatial-temporal propagation of concentration perturbation of attached hydrophobic particles to the bubbles in the pulp and froth zones after implementing the LQR. Figure 6 illustrates how an arbitrary initial profile is stabilized after approximately 12 minutes (which is the approximate residence time of the column). Even though an LQR was designed to provide exponential stability of the system from any initial condition in a finite dimensional setting, the transport-reaction system, which is infinite dimensional, has a finite time governed by the slowest state after which exponential stabilization can be achieved. Among all the states in the column, the one associated with the attached

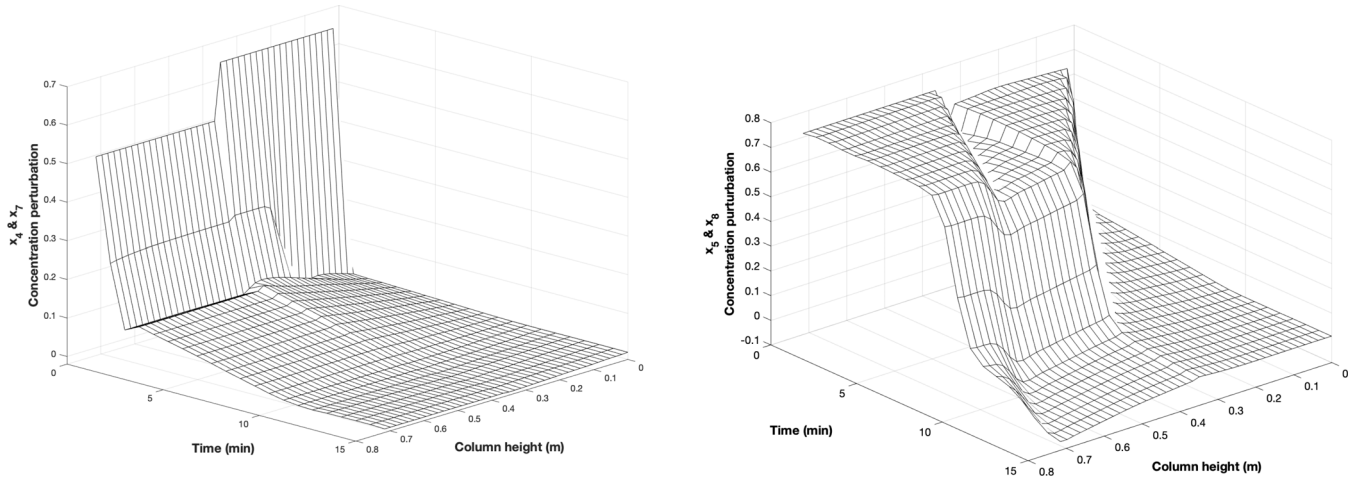

FIGURE 6 Concentration perturbation propagation of hydrophobic particles: free, x_4 and x_7, and attached, x_5 and x_8, in the pulp and froth

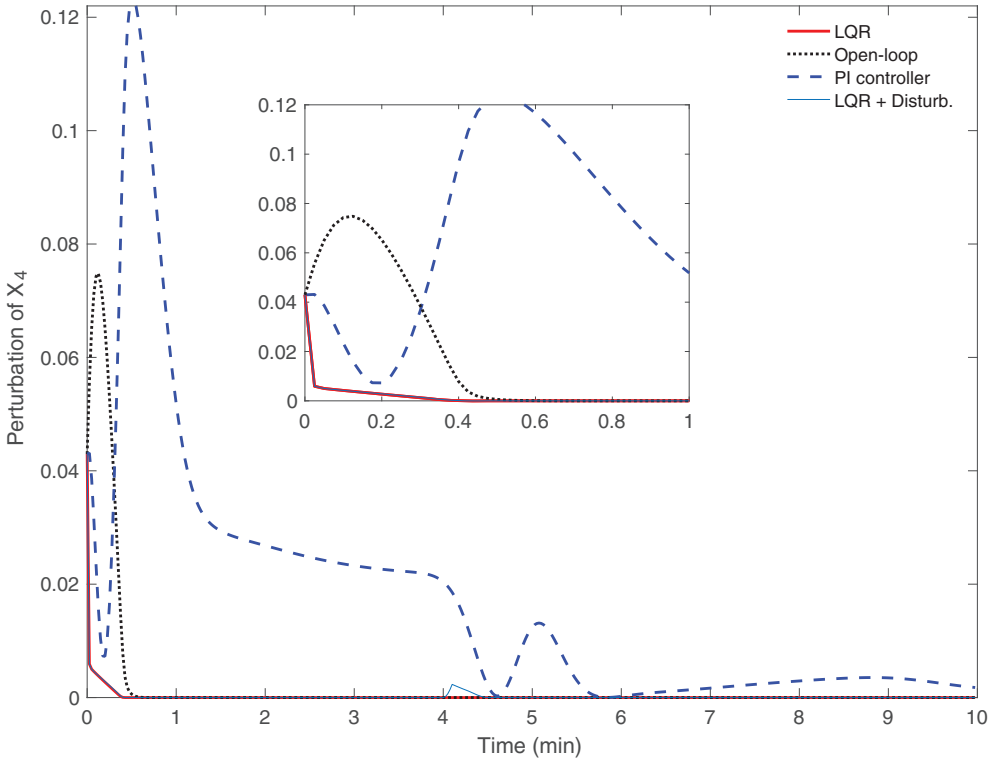

FIGURE 7 Integral of the squared concentration perturbation of free minerals in the up-flow in the pulp, $\int_{L_1}^{L_2} x_4^2(z,t)dz$: Thick line, linear quadratic regulator (LQR); dotted, open-loop; dashed, PI; thin line, LQR with disturbance applied at 4 minutes

particles to the bubbles, x_8, is the slowest state. Therefore, the dynamics of this state will define the finite time after which the controller stabilizes the system and brings the states to the steady state from any initial condition.

Two single input single output (SISO) proportional-integral (PI) controllers have been designed to work simultaneously to serve as a point of comparison for the LQR (multiple input multiple output PI control has not been considered here):

- PI_1: The controlled variable CV is the concentration of attached minerals at the top of the column, $x_8(L_2)$. The concentration of minerals in the feed, $X_{1,0}$, is selected as the measured variable MV. The selected controller gains are $K_c = 1$; $K_I = 0.01$ with the reference signal set to zero.
- PI_2: The CV is the concentration of free minerals in the down-flow at the bottom of the column, $x_3(0)$. The gas flow rate, Q_a, is selected as the MV, and controller

gains are $K_c = 0.5$; $K_I = 0.01$ with the reference signal set to zero.

To compare the rate of stabilization between different control design strategies, the squared norm of the state values has been integrated over the column height, which is an appropriate performance metric for this regulatory control problem. Figures 7-9 show the evolution of this norm for three representative states. For the case of free valuable particles in the pulp zone, the squared norm of the state perturbation has been integrated through the pulp height $\int_0^{L_1} x_4^2(z,t)dz$ and plotted over time in Figure 7. In the open-loop case, the system exhibits an inverse response, which is a characteristic of a linear system with a positive zero. It can be observed from Figure 7 that x_4, which represents the perturbation of the concentration of free valuable particles in the pulp zone, increases initially before it reaches the steady state. It is

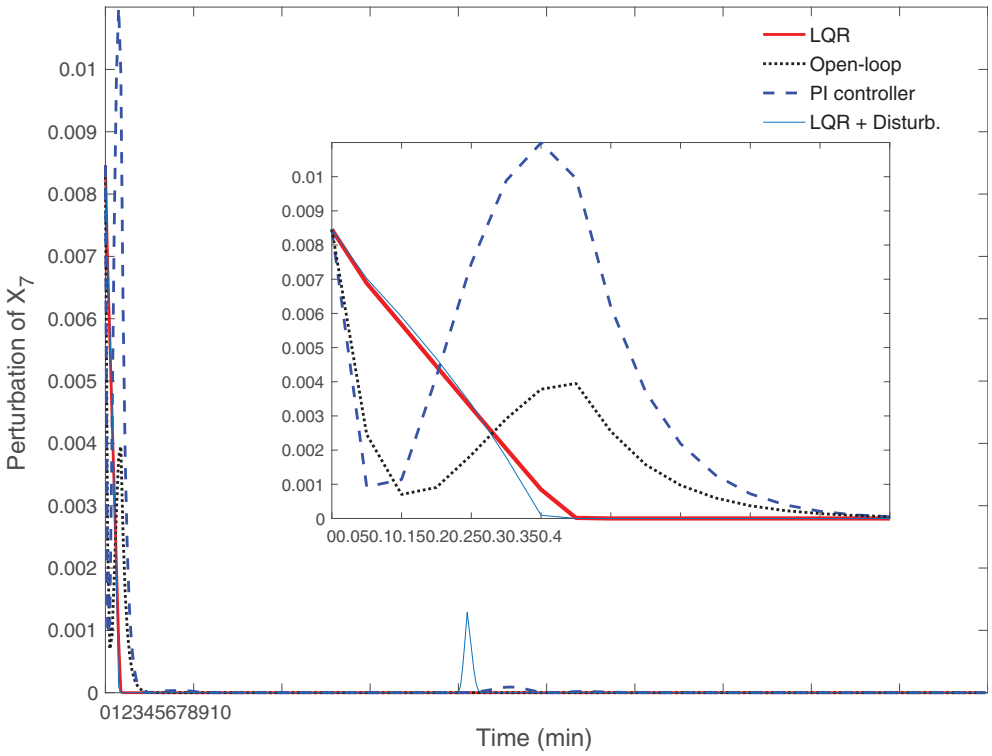

FIGURE 8 Integral of the squared concentration perturbation of free minerals in the up-flow in the froth, $\int_{L_1}^{L_2} x_7^2(z,t)dz$: Thick line, linear quadratic regulator (LQR); dotted, open-loop; dashed, PI; thin line, LQR with disturbance applied at 4 minutes

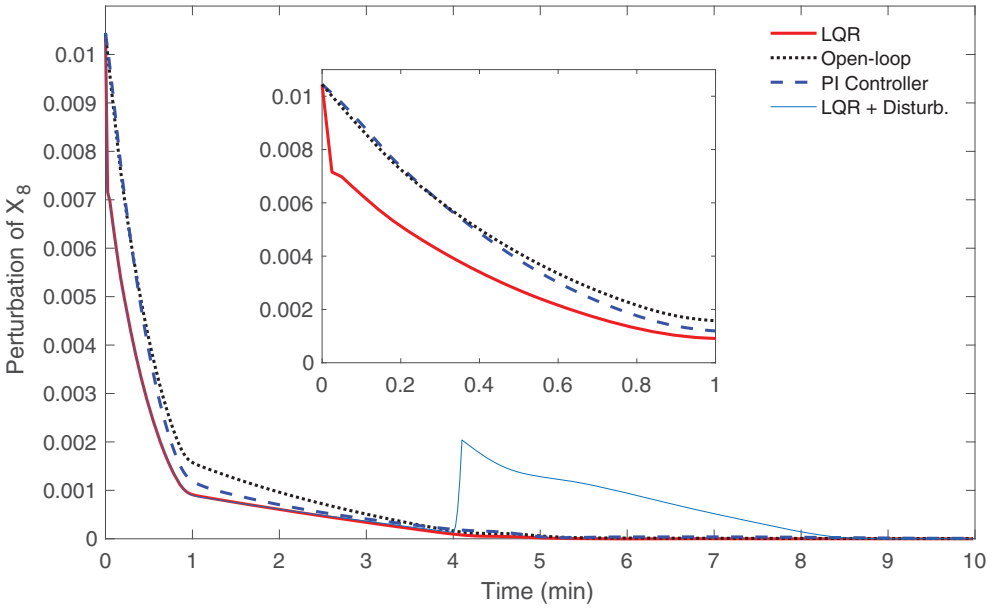

FIGURE 9 Integral of the squared concentration perturbation of attached minerals in the froth, $\int_{L_1}^{L_2} x_8^2(z,t)dz$: Thick line, linear quadratic regulator (LQR); dotted, open-loop; dashed, PI; thin line, LQR with disturbance applied at 4 minutes

expected that there is a dynamical interplay between the transport of x_4 in the up-flow along the column and the transfer of free particles between the downflow, upflow and the gas flows. The closed loop system with the PI controller has complex dynamics, as can be seen from Figure 7, with the perturbed state increasing and decreasing multiple times before reaching the steady state. A numerical comparison of the performance metric over the entire period of the simulation for Figure 7 shows that the metric is 2.25×10^{-3} for the LQR, 0.17 for PI control, and 2.06×10^{-2} for the open loop case. This means that the LQR stabilizes this state an order of magnitude faster than the open loop, and PI control performs worse on this count than even the open loop case. A similar comparison for Figure 8 shows the performance metric to be 7.20×10^{-4} for the LQR, 1.68×10^{-3} for the PI controller, and 8.05×10^{-4} for the open loop case.

As Figures 7-9, illustrate, the model-based controlled system has the ability to stabilize the initial condition faster than the non-model-based PI controlled system and the open-loop system. The state evolution goes to zero in finite time under the designed optimal control gain, but as was mentioned above, there is a minimum specific finite time (governed by the inherent time scale of the process), which is the fastest that the states can converge to the steady state. Although the LQR displays better performance than the open loop and the PI controller overall (see Figure 9), the difference in the case of x_8 (the slowest state) is not very significant. The performance metric in this case is 5.19×10^{-3} for the LQR, 9.80×10^{-3} for the PI controller, and 1.08×10^{-2} for the open loop case. Figures 7-9 also illustrate LQR controller rejection of disturbances in addition to robust stabilization of the system. A step disturbance has been applied to these states at 4 minutes. It can be seen that the delay rate in response to the initial perturbation is similar before and after the applied disturbance is rejected.

5 | CONCLUSIONS

A fundamental model based on physical principles has been proposed for a hybrid flotation column that includes an agitated section. The model considers bubble-particle attachment and detachment, includes relevant gas and liquid transport phenomena, consists of a set of coupled ODEs and transport hyperbolic PDEs, and goes beyond models proposed in the literature, where it was assumed that the column consists of a series of well-mixed CSTRs. Boundary linear quadratic regulation is developed for this system of coupled ODEs and PDEs, and this, too, extends the control formulation available in the literature, due to the complex structure of interconnection between transport flows and boundaries in the hybrid column. Through simulations, we demonstrate the efficacy of the optimal controller in stabilizing the column flotation system and show that it outperforms a non-model-based PI controller by more than an order of magnitude in terms of regulatory control response. Specifically, we demonstrate exponential stabilization by the LQR controller once the residence time of the system has passed, and also demonstrate the superior ability of the LQR controller to reject step disturbances while stabilizing the system robustly. We will address extension of this work to nonlinear model predictive control in future efforts to incorporate real-time implementation and constraint handling.

ACKNOWLEDGEMENTS

The authors gratefully acknowledge financial support from the Natural Sciences and Engineering Research Council of Canada through a Discovery grant. Vinay Prasad also acknowledges support from the Jaffer Professorship in Process Systems and Control Engineering in the Department of Chemical and Materials Engineering at the University of Alberta.

NOMENCLATURE

A_c	cross-sectional area of the column (m^2)
d_c	diameter of the column (m)
Db_n	bubble diameter in size class n (m)
G and m	attachment rate equation constants (dimensionless)
h , h_f	mass transfer coefficients of particles from upward to downward liquid flow in the pulp and froth, respectively (min^{-1})
h' , $h_{f'}$	mass transfer coefficients of particles from downward to upward liquid flow in the pulp and froth, respectively (min^{-1})
k	fraction of hydrophobic particles that goes to down-flow after the detachment in the pulp (dimensionless)
k_2	fraction of hydrophobic particles that goes to down-flow after the detachment in the froth (dimensionless)
K_{ac}	particle-bubble attachment rate constant in the well-mixed zone (min^{-1})
K_{ap3} and k_{ap4}	particle-bubble attachment rate constants of the free hydrophobic particles in the down-flow and up-flow in the pulp (min^{-1})
K_{di}	particle-bubble detachment rate constant in zone i (min^{-1})
K_{af6} and K_{af7}	particle-bubble attachment rate constants of free hydrophobic particles in the down-flow and up-flow in the froth, respectively (min^{-1})

L_1 height of the pulp zone on top of the well-mixed zone (m)
L_2 height of froth zone (m)
$l = L_1 + L_2$ the overall transport length of the pulp and froth zone (m)
Q_a air volumetric flow rate ($m \cdot min^{-1}$)
$Q_{e,i}$ upward liquid volumetric flow rate in i zone ($m \cdot min^{-1}$)
Q_f feed volumetric flow rate ($m \cdot min^{-1}$)
$Q_{r,i}$ downward liquid volumetric flow rate in i zone ($m \cdot min^{-1}$)
Q_t tailing volumetric flow rate ($m \cdot min^{-1}$)
Q_w wash water volumetric flow rate ($m \cdot min^{-1}$)
t time (minutes)
V_c volume of the CSTR zone (m^3)
$V_j(z)$ transport velocity of state j ($m \cdot min^{-1}$)
$v_{e,n,i}$ bubble velocity of bubble size class n in zone i ($m \cdot min^{-1}$)
X_1 and X_2 concentrations of free and attached hydrophobic particles in the CSTR ($kg \cdot m^{-3}$)
X_3 and X_4 concentrations of free hydrophobic particles in the liquid down-flow and up-flow in the pulp ($kg \cdot m^{-3}$)
X_5 and X_8 concentrations of attached hydrophobic particles in the pulp and froth ($kg \cdot m^{-3}$)
X_6 and X_7 concentrations of free hydrophobic particles in the liquid down-flow and up-flow in the froth ($kg \cdot m^{-3}$)
$X_{1,0}$ initial concentration of hydrophobic particles in the feed, which denotes the input into the CSTR ($kg \cdot m^{-3}$)
x perturbation of concentrations (states) around the steady state ($kg \cdot m^{-3}$)
z height, axial direction (m)
I liquid control volume in the CSTR
II gas control volume in the CSTR
III and III' liquid control volumes in the pulp zone regarding the down-flow and up-flow respectively
IV gas control volume in the pulp
V and V' liquid control volumes in the Froth zone regarding the down-flow and up-flow respectively
VI gas control volume in the froth
α_i percentage of the liquid phase in the down-flow (dimensionless)
$1 - \alpha_i$ percentage of the liquid phase in the up-flow (dimensionless)
δ a Dirac function
ε_i total gas holdup of the bubbles in zone i (dimensionless)
$\varepsilon_{i,n}$ gas holdup of the bubbles in size class n in zone i (dimensionless)
η the wash water input (kg/m^3)
$\rho_{l,i}$ slurry/liquid density (kg/m^3)
$\rho_{g,i}$ gas density (kg/m^3)

SUBSCRIPTS

c CSTR or well-mixed zone
d distributed parameter system (DPS)
f froth zone
i represents the zones (CSTR (c), pulp with plug flow (p), and froth (f))
l lumped parameter system (LPS)
p pulp zone
ss steady state

REFERENCES

[1] B. Wills, J. Finch, *Wills' Mineral Processing Technology: An Introduction to the Practical Aspects of Ore Treatment and Mineral Recovery*, Butterworth-Heinemann, Boston, MA **2015**.
[2] J. Finch, G. Dobby, *Column Flotation*, Pergamon Press, Oxford, UK **1990**.
[3] G. Mathieu, *CIM Bull.* **1972**, *65*, 41.
[4] M. C. Fuerstenau, G. J. Jameson, R. H. Yoon, *Froth Flotation: A Century of Innovation*, Society for Mining, Metallurgy and Exploration, Littleton, CO **2007**.
[5] J. Bouchard, A. Desbiens, R. D. Villar, *Miner. Eng.* **2005**, *18*, 709.
[6] F. Nakhaeie, A. Sam, M. R. Mosavi, *Arabian J. Sci. Eng.* **2013**, *38*, 1011.
[7] J. Bouchard, A. Desbiens, R. D. Villar, E. Nunez, *Miner. Eng.* **2009**, *22*, 519.
[8] I. Jovanović, I. Miljanović, *Arch. Min. Sci.* **2015**, *60*, 905.
[9] S. Gupta, P.-H. Liu, S. A. Svoronos, R. Sharma, N. Abdel-Khalek, Y. Cheng, H. El-Shall, *AIChE J.* **1999**, *45*, 557.
[10] K. Popli, M. Sekhavat, A. Afacan, S. Dubljevic, Q. Liu, V. Prasad, *Minerals* **2015**, *5*, 570.
[11] L. Wang, K. Runge, Y. Peng, C. Vos, *Miner. Eng.* **2016**, *98*, 187.
[12] A. Hassanzadeh, M. Firouzi, B. Albijanic, M. S. Celik, *Miner. Eng.* **2018**, *122*, 296.
[13] R. K. Tuteja, D. J. Spottiswood, V. N. Misra, *Miner. Eng.* **1994**, *7*, 1459.
[14] E. B. Cruz, *PhD dissertation*, Virginia Tech **1997**.
[15] K. S. Sastry, K. D. Lofftus, *Column Flotation* **1988**, *65*, 369.
[16] M. Bhole, J. Joshi, D. Ramkrishna, *AIChE J.* **2008**, *53*, 579.
[17] J. Yianatos, *Trans. Inst. Chem. Eng., Part A* **2007**, *85*, 1591.
[18] A. Saleh, *Physicochem. Probl. Mi.* **2010**, *44*, 215.
[19] R. Pal, J. Masliyah, *Can. J. Chem. Eng.* **1990**, *68*, 959.
[20] O. A. Bascur, *Developments in Mineral Processing*, Vol. 13, Elsevier, Rome, Italy **2000**, p. C8a.
[21] J. B. Yianatos, J. A. Finch, A. R. Laplante, *Int. J. Miner. Process.* **1986**, *18*, 155.
[22] A. Vazirizadeh, J. Bouchard, R. del Villar, *Miner. Eng.* **2015**, *74*, 207.
[23] A. Vazirizadeh, J. Bouchard, R. del Villar, M. Ghasemzadeh Barvarz, C. Duchesne, *Miner. Eng.* **2015**, *74*, 198.

[24] J. Bouchard, A. Desbiens, R. Del Villar, *Miner. Eng.* **2014**, *55*, 30.
[25] T. Yahui, M. Azhin, X. Luan, F. Liu, S. Dubljevic, *IFAC-PapersOnLine* **2018**, *51*, 99.
[26] R. Burger, S. Diehl, M. C. Marti, *J. Appl. Math.* **2019**, *84*, 930.
[27] J. E. Dickinson, K. P. Galvin, *Chem. Eng. Sci.* **2014**, *108*, 283.
[28] M. J. Mankosa, J. N. Kohmunench, G. H. Luttrell, J. A. Herbst, C. A. Noble, in *Int. Mineral Processing Congress*, Canadian Institute of Mining Metallurgy & Petroleum (CIM), Quebec City, Canada **2016**.
[29] A. Bensoussan, G. Da Prato, M. C. Delfour, K. Mitter, *Representation and Control of Infinite-Dimensional Systems*, Systems and Control: Foundations & Applications, Birkhauser, Boston, MA **2007**.
[30] A. A. Moghadam, I. Aksikas, S. Dubljevic, J. F. Forbes, *Automatica* **2013**, *49*, 526.
[31] H. K. Khalil, *Nonlinear Systems*, Prentice Hall, Englewood Cliffs, NJ **1991**.
[32] B. A. Francis, *SIAM J. Control Optim.* **1977**, *15*, 486.
[33] H. Knobloch, D. Flockerzi, A. Isidori, *Topics in Control Theory*, DMV Seminar Book Series, Birkhäuser Basel, Boston, MA **1993**.
[34] B. A. Francis, W. M. Wonham, *Appl. Math. Opt.* **1975**, *2*, 170.
[35] J. Deutscher, in *Proc. of the European Control Conf.*, IEEE, Linz, Austria **2015**, p. 891.
[36] A. Isidori, C. I. Byrnes, *IEEE Trans. Autom. Control* **1990**, *35*, 131.
[37] G. Dobby, J. Finch, *Chem. Eng. Sci.* **1985**, *40*, 1061.
[38] J. Yianatos, J. Finch, A. Laplante, *Trans. Inst. Min. Metall. Sect. C* **1987**, *96*, C199.
[39] K. V. S. Sastry, *I' Agglomeration-81*, NMA, Nuremberg, Germany, **1981**, pp. A122–A127.
[40] K. V. S. Sastry, D. W. Fuerstenau, *T. Soc. Min. Eng.* **1970**, *247*, 46.

How to cite this article: Azhin M, Popli K, Prasad V. Modelling and boundary optimal control design of hybrid column flotation. *Can J Chem Eng*. 2021;1–20. https://doi.org/10.1002/cjce.24010

APPENDIX A: ELEMENTS OF $\mathcal{F}$

Detailed expressions for the elements of $\mathcal{F}$ in Equation (95) are provided here:

$$F_{11} = -V_{6ss}\frac{\partial}{\partial z_f} + A_{311},\ F_{12} = A_{312},\ F_{13} = A_{313},$$
$$F_{15} = A_{312}\delta(L_1 - z)$$
$$F_{16} = A_{313}\delta(L_1 - z),\ F_{21} = A_{321} - A_{221}\delta(L_1 - z),$$
$$F_{22} = -V_{7ss}\frac{\partial}{\partial z_f} + A_{322}$$
$$F_{23} = A_{323},\ F_{24} = A_{323},\ F_{25} = -A_{221}\delta(L_1 - z)$$
$$F_{26} = -A_{222}\delta(L_1 - z) + A_{322}\delta(L_1 - z),$$
$$F_{31} = (A_{323} - A_{223})\delta(L_1 - z)$$
$$F_{32} = A_{331} - A_{231}\delta(L_1 - z),\ F_{33} = A_{332},$$
$$F_{34} = -V_{8ss}\frac{\partial}{\partial z_f} + A_{333}$$
$$F_{35} = -A_{231}\delta(L_1 - z),\ F_{36} = (A_{332} - A_{232})\delta(L_1 - z)$$
$$F_{41} = -A_{311}\delta(L_1 - z) + A_{211}\delta(L_1 - z),\ F_{42} = -A_{312}\delta(L_1 - z)$$
$$F_{43} = -A_{313}\delta(L_1 - z),\ F_{44} = -V_3\frac{\partial}{\partial z_p} + A_{211}$$
$$F_{45} = A_{212} - A_{312}\delta(L_1 - z),\ F_{46} = A_{213} - A_{313}$$
$$F_{51} = A_{221}\delta(L_1 - z),\ F_{54} = A_{221},\ F_{55} = -V_4\frac{\partial}{\partial z_p} + A_{222},$$
$$F_{56} = A_{223}$$
$$F_{61} = A_{231}\delta(L_1 - z),\ F_{64} = A_{231},\ F_{65} = A_{232},$$
$$F_{66} = -V_{5ss}\frac{\partial}{\partial z_p} + A_{233}$$

APPENDIX B: SIMULATION PARAMETERS

The unit simulated in this paper is a pilot plant flotation column with the following geometry: 0.72 m of height, 0.16 m in diameter. The simulation parameters for the quantitative study of the hybrid columnare as follows:

- CSTR: 0.56(*height*) * 0.16(*width*) * 0.16(*depth*)m^3
- Q_f: 0.1 m^3/min
- Q_t: 0.03 m^3/min
- Q_a: 0.0008 m^3/min
- Q_w: 0.001 m^3/min
- Q_{rp}: 0.0005 m^3/min
- Q_{rf}: 0.001 m^3/min
- Q_{ep}: 0.01 m^3/min
- Q_{ef}: 0.02 m^3/min
- k: 0.8; k_2: 0.75
- $G = 8.08$; $m = 0.45$
- K_{dc}: 0.0003 1/min

- K_{ap3}, K_{ap4}: 0.2 1/min
- K_{dp}: 0.005 1/min
- K_{af6}, K_{af7}: 0.05 1/min
- K_{df}: 0.01 1/min
- α_f: 0.1 1/min
- ε_c: (0.02,0.04,0.3)
- $D_{b,p}$: (0.0015,0.001,0.0005); ε_p: (0.08,0.24,0.08)
- $D_{b,f}$: (0.003,0.002,0.001); $\varepsilon_f = (0.18,0.46,0.06)$

A representative initial condition is $x_1(0) = 0.2$ kg/m^3, $xq_1(0) = 0.5$ kg/m^3, $x_2(0) = 0$.